Arabian Journal of Chemistry (2020) 13, 1975–1985

King Saud University

Arabian Journal of Chemistry

www.ksu.edu.sa
www.sciencedirect.com

ORIGINAL ARTICLE

Plasmonic and fluorescent sensors of metal ions in water based on biogenic gold nanoparticles

Luisa E. Silva-De Hoyos [a,b], Victor Sánchez-Mendieta [b], Miguel A. Camacho-López [c], Jésica Trujillo-Reyes [d], Alfredo R. Vilchis-Nestor [b,*]

[a] Facultad de Química, UAEM, Paseo Colón S/N, Residencial Colón, 50120, Toluca de Lerdo, Mexico
[b] Centro Conjunto de Investigación en Química Sustentable UAEM-UNAM, Km 14.5 Carretera Toluca-Atlacomulco, Campus Rosedal, Toluca de Lerdo, 50200, Mexico
[c] Laboratorio de Fotomedicina, Biofotónica y Espectroscopia Láser de Pulsos Ultracortos, Facultad de Medicina, UAEM, Av. Paseo Tollocan 134/502, Residencial Colón y Col Ciprés, 50120, Toluca de Lerdo, Mexico
[d] Department of Chemistry, The University of Texas at El Paso, 500 West University Ave., El Paso, TX 79968, USA

Received 25 November 2017; accepted 24 February 2018
Available online 6 March 2018

KEYWORDS

Gold nanoparticles;
Citrus paradisi;
Biogenic synthesis;
Plasmonic sensors;
Fluorescent sensors;
Metallic ions

Abstract Gold nanoparticles (AuNPs) were synthesized using a rapid, single step, and completely green biosynthetic method employing aqueous *Citrus paradisi* (grapefruit) extract, which was used as both the reducing and capping agent. Au(III) ions were rapidly reduced by the aqueous grapefruit extract, leading to the formation of highly stable and crystalline colloidal AuNPs, confirmed by the surface plasmon resonance (SPR) peak centered at 544 nm in the UV–Vis spectra. Biogenic AuNPs have been evaluated as plasmonic, fluorescent and naked-eye sensors of Pb^{2+}, Ca^{2+}, Hg^{2+}, Zn^{2+} and Cu^{2+} ions in aqueous media, with a good performance and selectivity. Of the three methods used for metal ions sensing, fluorescent sensors shows better results, specifically with Ca^{2+}, Cu^{2+} and Pb^{2+}. Copper was detected by both plasmonic and fluorescent methods.

1. Introduction

Noble metal nanoparticles (MNPs) made of gold, silver, platinum and palladium, are being widely used nowadays in medicine (Lohse and Murphy, 2012; Giljohann et al., 2010; Salata, 2004), biology (Giljohann et al., 2010; Salata, 2004), material science (Niemeyer, 2001), physics (Krueger, 2008) and chemistry (Handy et al., 2008), among others. They have exhibited unique physical, chemical, optical and thermo dynamical properties at nanometric regime, which leads them to many applications such as catalysis, sensors, biotechnology, and as surface-enhanced Raman scattering (SERS) as well (Prathnaa et al., 2011; Petla et al., 2012). Recently, the search for greener methods of synthesis has led to develop bio-inspired approaches. These methods have many advantages over the synthetic methods due to their cost effectiveness and

* Corresponding author.
E-mail address: arvilchisn@uaemex.mx (A.R. Vilchis-Nestor).
Peer review under responsibility of King Saud University.

Production and hosting by Elsevier

https://doi.org/10.1016/j.arabjc.2018.02.016
1878-5352

also because they do not involve the use of toxic chemicals, high pressure, energy and temperature (Prathnaa et al., 2011). Some of the bio-inspired systems employed in the synthesis of MNPs are constituted of bacteria (Das et al., 2014; Pantidos and Horsfall, 2014; Ghashghaei and Emtiazi, 2015), fungus (Pantidos and Horsfall, 2014; Ghashghaei and Emtiazi, 2015; Syed et al., 2013), and plant extracts (Pantidos and Horsfall, 2014; Mittal et al., 2013; Ahmed and Ikram, 2015). Plant extract mediated process is a versatile and simple method of synthesis for different types of MNPs such as Au, Pt, Pd, and Ag nanoparticles and metal oxides nanostructures (Jeevanandam et al., 2016).

Biosynthesis is currently considered as a good alternative for the designing of greener, safe and environmentally friendly protocols for the synthesis of NPs compared to the conventional physical and chemical processes (Petla et al., 2012; Sharma et al., 2019; Dauthal and Mukhopadhyay, 2016; Hebbalalu et al., 2013). The use of waste materials not only reduces the cost of synthesis, but also minimizes the need of using hazardous chemicals, which encourages "green synthesis".

The biosynthesis of NPs has been suggested to occur through electrostatic and ionic interactions between the metal complexes and the functional groups on the biomass (plant extract). There are several organic compounds in plant systems such as flavonoids, terpenoids, proteins, reducing sugars and alkaloids that can be involved as either reducing or capping agents during the synthesis (Gan and Li, 2012; Yoosaf et al., 2007). The concentration of the compounds found in the biomass can be related with the shape and size of nanoparticles (Sinha et al., 2009; Gan and Li, 2012; Montes et al., 2011; Bankar et al., 2010; Romo-Herrera et al., 2011).

For instance, it has been reported that the synthesis of triangle-shaped AuNPs, is the result of the interaction between the metal nanoparticle with the functional groups of the aldehydes and ketones present in the *Citrus paradisi* plant extract, while the reduction of the precursor salt ($HAuCl_4$) is linked to the —OH moieties present in biomolecules such as sugars and polyphenols (Sinha et al., 2009). In addition, the pH, temperature, reaction time, and amount of extract, are imperative factors during the biosynthesic process (Gan and Li, 2012; Montes et al., 2011).

Gold nanotriangles might grow by a rapid reduction and the addition of large amount of biomolecules; so the reductive biomolecules dictated the formation of gold nanotriangles. Due to the large amount of reductive biomolecules, all the nuclei of gold species form at the same time at the beginning of the reduction with almost none nucleation of smaller particles. As a consequence, the nucleation process is fast, but the growth is slow, resulting in gold nanotriangles. With *Citrus paradisi* extract the biomolecule known as narangin may be the one that dictates the formation of the gold nanoparticles (Huang et al., 2007).

Because of their simple preparation, physical and chemical properties, and high surface area, the nanoparticles are one of the most promising nanotechnology approaches on the way to obtain materials to be employed as sensors. The nanomaterials with a great potential to build-up sensors could be the MNPs, as they are able to display localized superficial plasmon resonance (LSPRs) (Noguez, 2005; González et al., 2005). The LSPRs of AuNPs lie within the visible and near infrared range of the electromagnetic spectrum. Therefore, these type of NPs are suitable as optical sensors.

Several researchers have stated that the resonance frequency depends on the size, geometry, composition, and environment of the MNPs (Noguez, 2005; González et al., 2005; Langer et al., 2015; Polavarapu et al., 2014). For example, the most remarkable effect of localized plasmon resonance is the strong electromagnetic near-field enhancement, also known as FE, which has up to several orders of magnitude and is localized at a nanometer scale (Langer et al., 2015). FE plays one of the major roles in absorption, reflection, Raman scattering and fluorescence processes of molecules located near metal NPs. This phenomenon has high relevance also for sensor applications (Langer et al., 2015; Polavarapu et al., 2014).

In order to obtain the fluorophore emission, the electrons need to be exited from ground state to excited state with electromagnetic radiation. These emissions can be altered when the fluorophore is placed with an entity that possesses an electromagnetic field, such as the surface plasmon resonance (SPR). It has been observed that MNPs can be considered as good candidates for this kind of entity, upon receiving optical energy (Yue et al., 2015). When the fluorophore is at a short distance from the metal nanoparticle, the electrons of the fluorophore that are participating in the excitation/emission can interact with the field of the nanoparticle. This interaction results in the change of the fluorescence emission level, quenching or enhancement (Yue et al., 2015; Kang et al., 2011; He et al., 2008).

Kang et al. (2011) has reported that the main factors that affect the fluorescence by a metal nanoparticle could be: (1) The plasmonic field produced around the particle by an incident light, increases the excitation-decay rate of the fluorophore, which also enhances the level of fluorescence emission; and (2) The dipole energy around the nanoparticle reduces the ratio between radiative and non-radiative decay, as well as the quantum yield of the fluorophore, resulting in the fluorescence quenching (Kang et al., 2011).

Therefore, the aim of this work is to present a one-pot biosynthesis of AuNPs using different amounts of *Citrus paradisi* (grapefruit) extract and their influence on the morphological ratio between spherical:planar nanoparticles. Also, to study their application as plasmon resonance sensors for Hg^{2+}, Ca^{2+} and Zn^{2+} species and fluorescent sensors for Ca^{2+}, Cu^{2+} and Pb^{2+} moieties existing in water.

2. Materials and methods

2.1. Materials

Citrus paradisi was obtained from a local store. $HAuCl_4$, Rhodamine 6G (Rh6G), calcium(II) chloride ($CaCl_2$), copper(II) chloride ($CuCl_2$) and lead(II) chloride ($PbCl_2$), were acquired as analytical grade reagents from Sigma-Aldrich. All chemicals were used without any further purification. Deionized water was employed in all the steps of the synthesis.

2.2. Preparation of Citrus paradisi extract

The grapefruit was washed with water. The peel was cut, weight (90 g) and boiled for 20 min in 90 mL of deionized water; upon cooling the infusion was vacuum-filtered. The resulting aqueous extract was stored on a flask at room temperature for an hour and used for further experiments as the bioreducing agent (Nolasco-Arizmendi et al., 2012; Li et al., 2008).

2.3. Biosynthesis of Au-NPs

The biological synthesis of gold nanoparticles was carried out by using 5 mL of a 10^{-3} M $HAuCl_4$ solution and pouring 2, 3 or 4 mL of *Citrus paradisi* extract, respectively. This synthesis is an adaptation of a method previously reported (Nolasco-Arizmendi et al., 2012; Li et al., 2008).

2.4. Characterization of Au-NPs

UV–Vis spectroscopy was performed using a Lambda 650 Perkin-Elmer spectrophotometer.

For transmission electron microscopy (TEM) analyses, the samples were prepared by placing drops of the reaction mixture over carbon-coated grids and allowing evaporation. TEM observations were performed on a JEOL 2100 microscope operated at 200 kV of accelerating voltage with a LaB_6 filament. For calculating the distribution size of nanoparticles in one sample, at least 25 representative micrographs were taken for each sample, and approximately 400 nanoparticles per sample were considered for measurements. Particle size diameters were calculated with the equation $d_{avg} = P(n_i d_i)/Pn_i$, where n_i is the number of particles of diameter d_i.

2.5. Fourier transform infrared spectroscopy (FTIR) analysis

Both the grapefruit extract and the biogenic AuNps were left to dry at room temperature for 48 h. They were analyzed by using a Bruker spectrophotometer Tensor 27 with MIR source, ATR accessory (model ATR Platinum) and diamond crystal. An aliquot of 40 mL of the grapefruit extract and the biogenic AuNps solution were separately allowed to dry at room temperature. The powder obtained was tested by the spectrophotometer for solids.

2.6. Sensing

Sensing studies were performed with the AuNPs synthesized using 2 mL of reducing agent (*Citrus paradisi* aqueous extract). An aliquot of 1 mL of each 10^{-3} M aqueous solutions of Mg^{2+}, Hg^{2+}, Sr^{2+}, Pb^{2+}, Ca^{2+}, Cu^{2+} and Zn^{2+} were added to 1 mL of the AuNPs suspension at room temperature. The sensing performance and selectivity towards the Pb^{2+}, Ca^{2+} and Cu^{2+} metal ions by the AuNPs suspension were tested by using the UV–Vis and fluorescence spectroscopies. Initially, 1 mL of Rh6G (10^{-6} M) was gradually added to 1 mL of biogenic AuNPs and stirred for 30 min. After that, 1 mL of 10^{-3} M of Cu^{2+}, Ca^{2+} and Pb^{2+} aqueous solutions were added separately to the solution. The performance of AuNPs with Rh6G as sensor was monitored using a Horiba Jobin-Ivon, FluoroMax-P spectrofluorometer.

3. Results and discussion

3.1. Synthesis and characterization of AuNPs

The addition of *Citrus paradisi* aqueous extract to a 10^{-3} M aqueous $HAuCl_4$ solution led to the appearance of a dark purple color in the solution after one hour of reaction. This color change indicates the AuNPs formation. Fig. 1A shows the characteristic surface plasmon resonance band of AuNPs centered between 540 and 544 nm in the UV–Vis absorption spectra. It can be observed that as the reaction time advances, the absorbance intensity increases. This also can be related with a greater number of formed NPs due to the behavior on the UV–Vis spectra profiles, which are characteristic of aggregated nanoparticles (Shipway et al., 2000) or anisotropic nanostructures when changing dimensions during the time (Shiv Shankar et al., 2005). Inset on Fig. 1A shows an image of the NPs suspensions at different times during the reaction of 2 mL of *Citrus paradisi* extract and 5 mL of a 10^{-3} M $HAuCl_4$ solution. The large color variations oscillate in ranges from light yellow to dark purple as the time passes. In this figure, the colloidal solutions display color changes due to the excitation of the surface plasmon vibrations in AuNPs (Song and Kim, 2009). In addition, it is well known that the width and shift of the plasmon band can be also associated to the shape and size of the NPs, respectively (Noguez, 2005; González et al., 2005).

Fig. 1B shows the UV–Vis absorbance spectra of AuNPs synthesized with different amounts of *Citrus paradisi* aqueous extract and recorded after 24 h of reaction. The spectra 1 (540 nm), 2 (549 nm), and 3 (568 nm) correspond to 2 mL, 3 mL, and 4 mL of extract, respectively. All the AuNPs exhibited a strong absorbance bands. However, as the amount of *Citrus paradisi* extract increases in the reaction medium, the band shifts to a larger wavelength weakening its intensity. This behavior could be attributed to the increase of NPs size. This behavior agrees with the studies of González et al. (2005) and Langer et al. (2015). They theoretically and experimentally proved that the plasmon oscillation of metal nanoparticles are optically coupled to each other when they are brought in proximity (Noguez, 2005; Langer et al., 2015; Yoosaf et al., 2007).

Fig. 2A and C shows the UV–Vis absorbance spectra of AuNPs that have been synthetized by reacting aqueous $HAuCl_4$ with 3 mL and 4 mL of *Citrus paradisi* extract at different times, respectively. The presence of the surface plasmon resonance indicates the reduction of gold ions by the aqueous *Citrus paradisi* extract in order to form the nanoparticles, which were verified by the Transmission Electron Microscopy (TEM). The micrographs showed the formation of gold nanoplates (triangles and hexagons), and also smaller spherical-shaped NPs (Figures B and D). It was also observed that unlike the triangular-shaped NPs, when the amount of aqueous extract increases, the size of the spherical-shaped NPs also increases (Fig. 2B, D). The size range of the spherical AuNPS was between 10 and 90 nm (Fig. 2B), while the range edge length of hexagonal and triangular AuNPs was estimated to be between 75 and 325 nm (Fig. 2D). According to Shiv Shankar et al. (2005) if the amount of extract added to the $HAuCl_4$ solution increases, the average size of the triangular and hexagonal particles decreases, and the ratio of the number of spherical nanoparticles to triangular/hexagonal particles increases with a larger amount of extract (Shiv Shankar et al., 2005).

As can be observed in Fig. 2, with the increment of the extract volume employed for the synthesis, a shift of the absorbance band is observed, which can be related to changes of the particle shape and size. This behavior was also reported by Ahmed et al. (2016).

Fig. 3 shows the TEM micrographs of the synthesized AuNPs using different amounts of *Citrus paradisi* aqueous

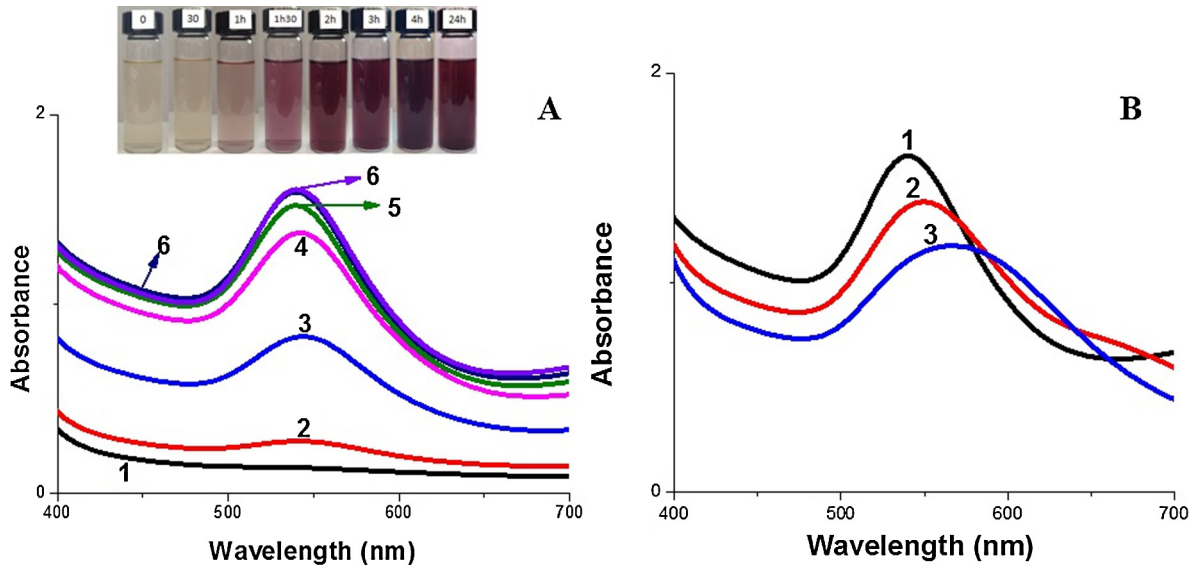

Fig. 1 (A) UV–Vis spectra of biogenic AuNPs measured at different times during the reaction of 2 mL of *Citrus paradisi* extract with 5 mL of a 10^{-3} M $HAuCl_4$. Curves profiles correspond to 1 (30 min), 2 (1 h), 3 (1.5 h), 4 (2 h), 5 (4 h), and 6 (24 h), respectively. (Inset) Image of AuNPs obtained at different reaction times. (B) UV–Vis spectra of biogenic AuNPs formed after 24 h of reaction of 5 mL of a 10^{-3} M $HAuCl_4$ with different amounts of *Citrus paradisi* extract. Spectra 1, 2 and 3 correspond to 2 mL, 3 mL, and 4 mL of *Citrus paradisi* extract, respectively.

extract: 2 mL (Fig. 3A and B), 3 mL (Fig. 3C and D), and 4 mL (Fig. 3E and F). It can be seen that by increasing the amount of aqueous extract in the reaction medium, the polydispersity decreases, and the morphology of AuNPs change.

The TEM analysis Fig. 3A and B, reveal the formation of spherical, hexagonal planar, and larger triangular nanoparticles with dimensions between 25 and 325 nm.

However, as the amount of *Citrus paradisi* aqueous extract is increased to 3 mL in the reaction medium, the sample shows a higher percentage of planar-shape leading to the formation of triangle-shape (Fig. 3C, D). The same trend is also followed when the amount of extract is increased to 4 mL (Fig. 3E and F). This tendency is clearly reflected in the UV–Vis absorbance spectra in Fig. 1B, which shows an increase in the intensity and a bathochromic shift of the band.

With the increase of triangular AuNPs in the solution, the maximum absorbance undergoes a bathochromic shift. This behavior can be correlated with the results of the UV–Vis spectra showed in Fig. 2A (red-2 and blue-3) (Noguez, 2005; González et al., 2005; Shiv Shankar et al., 2005). The bathochromic shift (red shift) can be related to shape of the nanoparticles; or it can also be associated with nanoparticles with fewer faces and sharper vertices (Noguez, 2007).

On the other hand, the single crystalline nature of the biogenic AuNPs is revealed in the selected area electron diffraction (SAED) rings. Fig. 4A shows the SAED of the AuNPs synthesized by using 2 mL of *Citrus paradisi* aqueous extract. The diffraction rings on the image could be indexed based on the face centered cubic (FCC) structure of gold, and are assigned to the family planes {1 1 1}, {2 0 0}, {2 2 0} and {3 1 1}, respectively (Germain et al., 2003). Fig. 4B and C also presents the ring-like diffraction pattern, which indicates that the particles are crystalline. The diffraction rings could also be indexed based on the FCC structure of gold assigned to the family planes {1 1 1}, {2 2 0}, {3 1 1} and {4 0 0} for the AuNPs synthesized with 3 mL of *Citrus paradisi* aqueous extract; while the family planes {1 1 1}, {2 0 0}, {2 2 0} and {3 1 1} correspond to the AuNPs synthesized with 4 mL of plant extract.

Germain et al., (2003) states that "A unique (1 1 1) stacking fault model which is parallel to the flat (1 1 1) disk surface has been proposed to explain the observed 1/3{4 2 2} forbidden reflections in [1 1 1] SAED pattern and the corresponding 3-{4 2 2} image". Therefore, the hexagonal arrange of the diffraction spots indicate that gold nanoprisms are highly [1 1 1] oriented with the top normal to the electron beam, and the presence of the 1/3{4 2 2} Bragg reflection (squared box spot) shows the flat nature of the gold nanostructures, as can be observed in the SAED patterns of Fig. 4 (Shiv Shankar et al., 2004; Germain et al., 2003).

Additionally, further studies have shown that the presence of defects (twin planes) leads to the formation of anisotropic metal nanoparticles, such as planar triangles and hexagons (Lefton and Sigmud, 2005). In a similar way, it is possible that multiple twinned particles (MTPs) that are initially formed in the reaction, undergo a shape transformation and evolve into Au nanotriangles or hexagonal particles because of the shape-directing effect of the constituents of the *Citrus paradisi* extract (Wiley et al., 2005; Prathap Chandran et al., 2006). This phenomenon of growth can be seen in our system since the ratio between spherical:planar particles directly depends on the quantity of *Citrus paradisi* extract used in the synthesis. It was also observed that with a greater amount of extract, the amount of spherical NPs slightly decreases from 84% to 81%, while the proportion of planar particles increases from 8% to 18%. In addition, the size of the spherical NPs increases from 5 nm to 10 nm when using higher amounts of aqueous extract, while the size of the nanotriangles decreases from 75 nm to 25 nm.

The grapefruit aqueous extract and the colloidal suspension containing the biogenic AuNPs were characterized by FTIR spectroscopy. The major constituents of these peels are

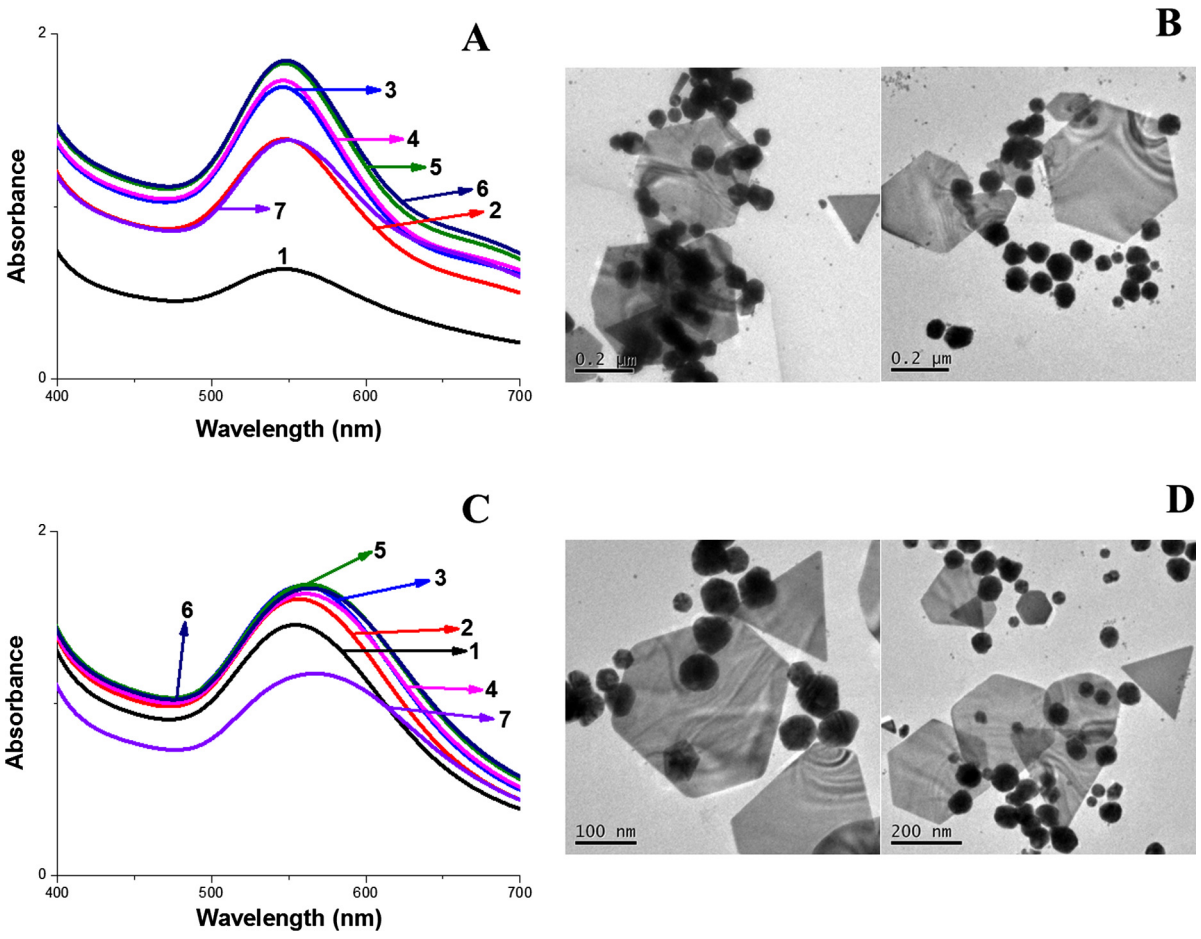

Fig. 2 (A) UV–Vis spectra of biogenic AuNPs measured at different times during the reaction of 3 mL of *Citrus paradisi* extract with 5 mL of a 10^{-3} M $HAuCl_4$ solution. Curves profiles correspond to 1 (30 min), 2 (1 h), 3 (1.5 h), 4 (2 h), 5 (4 h), and 6 (24 h), respectively. (B) TEM micrographs of AuNPs of 3 mL of *Citrus paradisi* extract with 5 mL of a 10^{-3} M $HAuCl_4$ solution. (C) UV–Vis spectra of biogenic AuNPs measured at different times during the reaction of 4 mL of *Citrus paradisi* extract with 5 mL of a 10^{-3} M $HAuCl_4$. Curves profiles correspond to 1 (30 min), 2 (1 h), 3 (1.5 h), 4 (2 h), 5 (4 h), and 6 (24 h), respectively. (D) TEM micrographs of AuNPs of 4 mL of *Citrus paradisi* extract with 5 mL of a 10^{-3} M $HAuCl_4$ solution.

protein, pectin, cellulose, and pigments (Nolasco-Arizmendi et al., 2012). Usually, the broad band located at 3640–3510 cm^{-1} corresponds to the stretching bond O—H of an alcohol or a phenol moiety. The band located between 3000 and 2800 cm^{-1} corresponds to stretching vibrations of C—H, while the bands observed in the region of 1747 cm^{-1} and 1647 cm^{-1} are usually endorsed to the stretching vibrations of COO^- and C═O, respectively. The bands that appear around 1300–1000 cm^{-1} (circled in blue on the two spectra of Fig. 5) can correspond to the vibrations of C—O—C and O—H in the polysaccharides (Nolasco-Arizmendi et al., 2012; Li et al., 2008). These molecules may be the ones that help in the reduction and interact with the metal ions (causing different symmetrical and asymmetrical vibrations depending on the anchorage) (Nestor, 2006).

3.2. Plasmonic colorimetric studies

The plasmonic colorimetric assays are based on the color change that occurs in the NPs solutions when there is a shift in the plasmonic response due to the interactions between the NPs and certain analytes such as biomolecules. The AuNPs have a high extinction cross section in the visible region of the electromagnetic spectrum that made them suitable for colorimetric assays based on naked-eyed detection. Some advantages of this kind of detection are that it is instrument free, simple, sensitive, selective, portable, and fast, characteristics that can be applicable to a wide range of analytes, in the clinical, biological and environmental arena (Polavarapu et al., 2014). In addition, the introduction of metal ions in a biogenic noble metal NPs solution can induce their aggregation through the carboxylic groups of the biomolecules present in the surface of the NPs and ions. This metal-ligand interaction can cause a color change (Polavarapu et al., 2014; Ding et al., 2010) making visible the presence of metal ions.

Fig. 6A and B shows the UV–Vis spectra of AuNPs synthesized with 2 mL of *Citrus paradisi* extract and the image of AuNPs solutions after being in contact with several metal ions, respectively. It can be observed that the addition of different metal ions such as Mg^{2+}, Hg^{2+}, Sr^{2+}, Pb^{2+}, Ca^{2+}, Cu^{2+} and Zn^{2+} to the AuNPs system had a small color change from

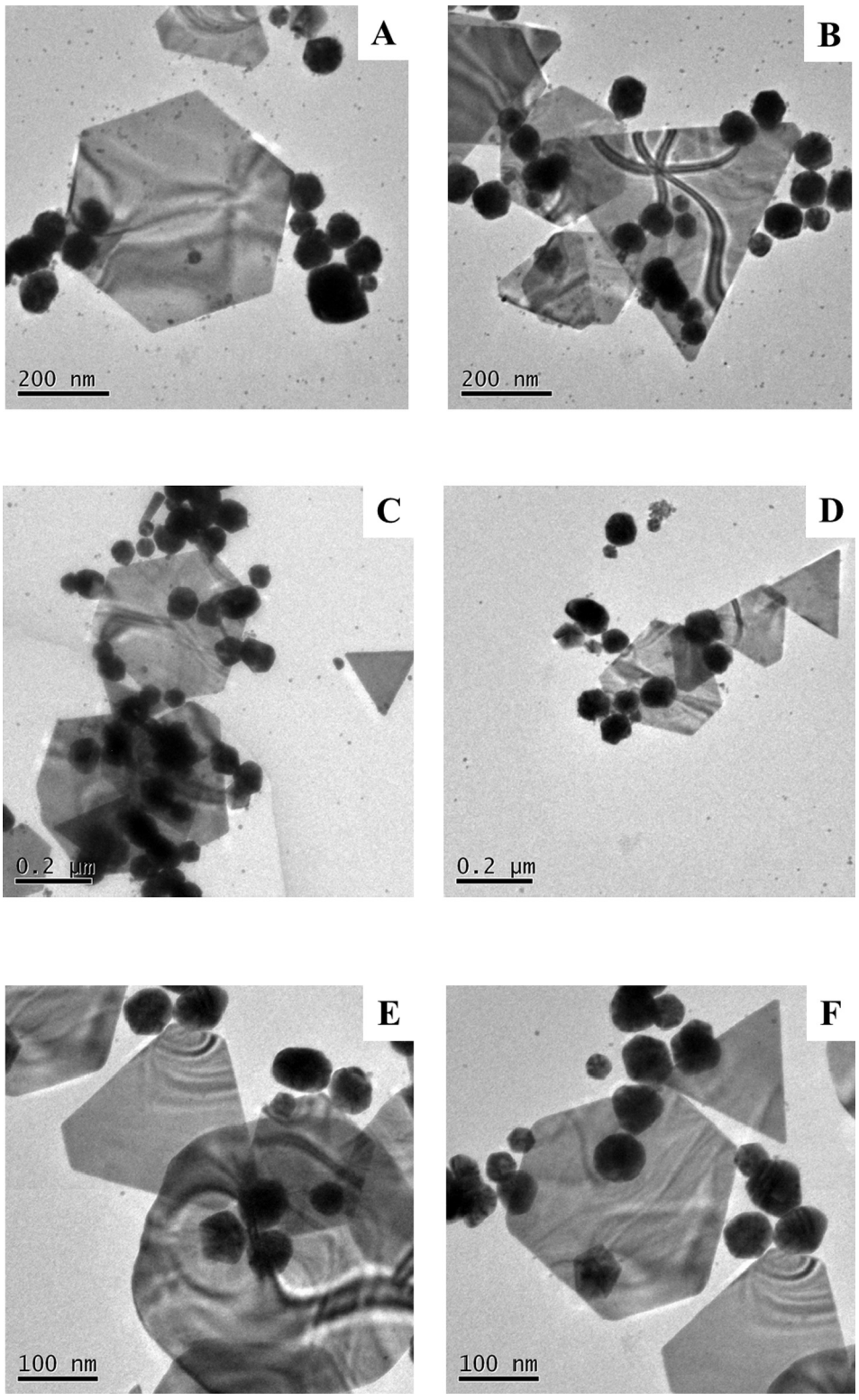

Fig. 3 (A–B), (C–D), (E–F) Representative TEM micrographs of biogenic AuNPs measured at different reaction volumes of 2, 3 and 4 mL of *Citrus paradisi* extract with 5 mL of a 10^{-3} M $HAuCl_4$, respectively.

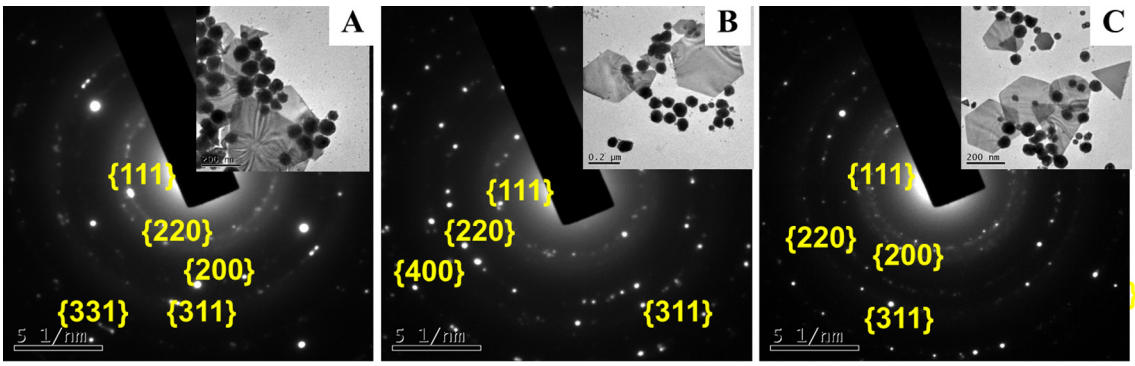

Fig. 4 SAED pattern of biogenic AuNPs collected after 24 h of reaction using 5 mL of a 10^{-3} M $HAuCl_4$ solution with (A) 2 mL, (B) 3 mL and (C) 4 mL of *Citrus paradisi* aqueous extract, respectively. Insets in each SAED pattern show TEM micrographs of the corresponding biogenic AuNPs.

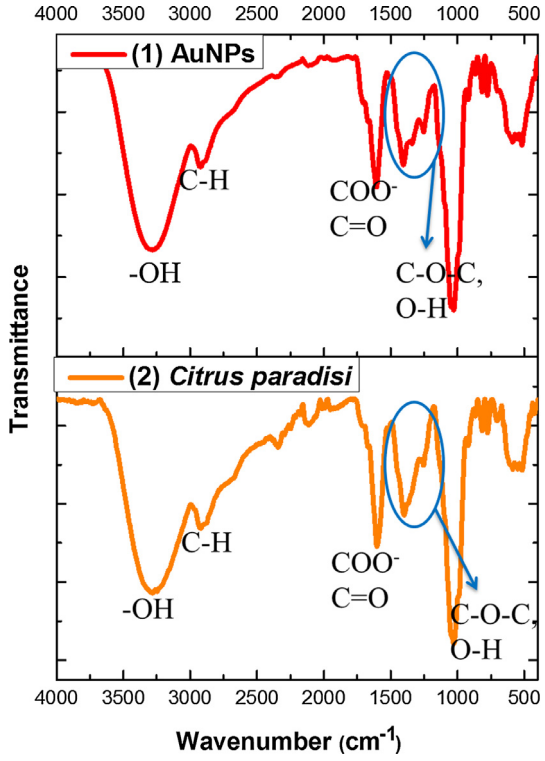

Fig. 5 (1) FTIR spectrum of colloidal suspension of biogenic AuNPs obtained from the reaction of 2 mL of *Citrus paradisi* extract and 5 mL of a 10^{-3} M $HAuCl_4$solution, (2) FTIR spectrum of *Citrus paradisi* aqueous extract.

dark purple to light purple. In this case, the surface plasmon sensing and fluorescent sensing had better response (Fig. 6B).

3.3. Surface plasmon sensing

Localized Surface Plasmon Resonances (LSPR) sensing frequencies depend on the environment, inter-particle distance, size, shape and composition of the NPs (Noguez, 2005; González et al., 2005; Langer et al., 2015). These parameters have been explored for LSPR sensing applications (Langer et al., 2015). Sensing strategies via shifts or changes in LSPR are considered attractive because of the simple implementation, easy handling of the instrument, and the eco-friendlier method. For instance, Langer et al. (2015) reported that surface plasmons can be measured by an extinction spectrum using UV–Vis spectroscopy. Therefore, the nanoplasmonic sensors can directly work in aqueous solutions. A phenomenon called 'dimer' appears when two individual nanoparticles are close to each other and become optically coupled due to the interaction of their dipoles. The coupled dimer exhibits and additional resonance with a lower energy which depends on the gap between the particles. With a smaller gap, the electric field becomes stronger and confined, which leads to a larger red shift of the plasmon resonance mode, observed by a color change (Langer et al., 2015).

The polyphenolic compounds that can be present in the aqueous extract of *Citrus paradisi* are known to form complexes with heavy metal cations. The addition of the metal ions to the AuNPs suspension results in a light bathochromic shift in the SPR band (Fig. 6A). For instance, with the addition of Zn^{2+}, the shift of the band goes from 554 nm to 546 nm; with Cu^{2+} and Hg^{2+} moves from 554 nm to 557 nm. According to Yoosaf et al., the extent of the shift depends on the concentration of ions in the solution or the type of aggregates that are formed with each metal ion (Yoosaf et al., 2007). The bathochromic shift in the SPR band and the visual color change (Fig. 6A and B) could be attributed to the formation of smaller aggregates of NPs in the presence of metal ions such as Hg^{2+}, Cu^{2+}, and Zn^{2+}.

The addition of different metal ions (Mg^{2+}, Hg^{2+}, Sr^{2+}, Pb^{2+}, Ca^{2+}, Cu^{2+} and Zn^{2+}) to the system after the AuNPs biosynthesis using 2 mL of *Citrus paradisi*, causes a moderate color change of the original colloidal solution. The color change goes from purple to light purple, enough to differentiate between the metallic ions tested by naked-eyed inspection.

It has been experimentally proven that the plasmon oscillation of metal NPs can be coupled to each other when they are brought in proximity (Langer et al., 2015; Yoosaf et al., 2007). In this work, the proximity of the NPs induces the coupling of their SPR, resulting in the shift to higher wavelengths (bathochromic shift). This behavior was visible with the addition of Hg^{2+}, Cu^{2+} and Zn^{2+} to the AuNPs solution (Fig. 6A).

Fig. 7 shows a schematic model of the formation of nanoparticle-ligand (capping agent)-metal ion that leads to the AuNPs aggregation. This figure can explain the color

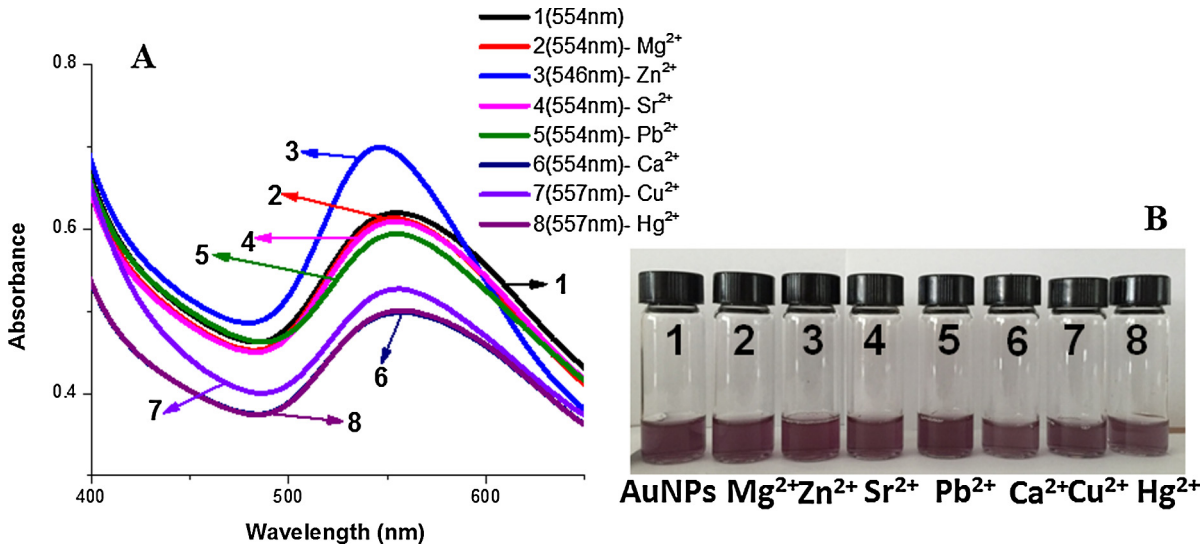

Fig. 6 (A) UV–Vis spectra of biogenic AuNPs synthesized with 5 mL of a 10^{-3} M $HAuCl_4$ solution and 2 mL of *Citrus paradisi* extract when tested as sensors of several metal ions (Mg^{2+}, Hg^{2+}, Sr^{2+}, Pb^{2+}, Ca^{2+}, Cu^{2+} and Zn^{2+}). (B) Image of AuNPs suspensions after being in contact with a 10^{-3} M aqueous solution of Mg^{2+}, Hg^{2+}, Sr^{2+}, Pb^{2+}, Ca^{2+}, Cu^{2+} and Zn^{2+} (1:1 v/v).

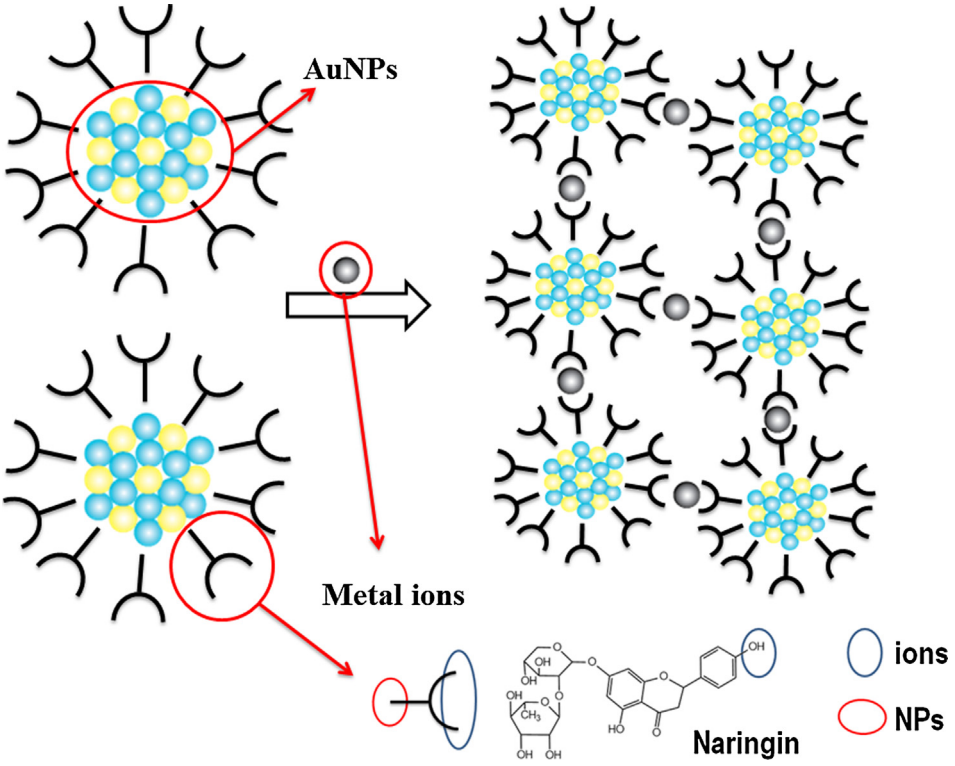

Fig. 7 Schematic representation of the formation of the metal-ligand complex leading to NPs' aggregation.

change in the solutions (Fig. 6B) and the behavior presented in Fig. 6A.

3.4. Fluorescence sensing

Fluorescence spectroscopy is usually used for sensing applications due to the high cross section of the emission process. This emission can be affected when a dye molecule is near a plasmonic nanoparticle, giving the NPs better properties in sensing applications. Fluorescence emission properties are not always enhanced by SPR, but the distance between the fluorophore and the NPs surface determines the effect, which ranks from quenching up to enhancement (Langer et al., 2015).

In this study, AuNPs-Rh6G complex was tested as probe for detection of different metal ions. Joseph Kirubaharan et al. (2012) has indicated that the involved heavy metal

perception mechanism could occur in two steps: (1) fixation of Rh6G dye molecule over the surface of the biogenic gold nanoparticle and, (2) replacement of the dye by metallic ions. Therefore, the released dye molecule acts as a visual colorimetric sensor. For example, Rh6G dye exhibits a pink color, while the AuNPs exhibits a purple color (Fig. 8B vial 1). When the Rh6G is attached to the biogenic AuNPs, the solution changes to a pink-brownish color (Fig. 8B vial 2). However, with the addition of the metal solutions (calcium (II) chloride, copper (II) chloride and lead(II) chloride) which provide Ca^{2+}, Cu^{2+} and Pb^{2+} ions, respectively, there is not a visual color change. These ions can start to adhere on the surface of the AuNPs by replacing some of the Rh6G dye molecules. Then, the fluorescent detection has a better result because the color change is not remarkable (Joseph Kirubaharan et al., 2012).

Sensing studies were further evaluated using a fluorescence spectrometer, where the Rh6G fluorophore exhibited a strong fluorescent emission peak (Fig. 8A-peak 1). When the Rh6G was added to the AuNPs solution and attached to the surface of the NPs, the spectrum presented a quenching in the fluorescent emission (Fig. 8A-peak 2) through the fluorescence resonance energy transfer which could promote also a small blue shift of around 20 nm. After the addition of 1 mL of 10^{-3} M solution of metal ions (Ca^{2+}, Cu^{2+} and Pb^{2+}), the fluorescence emission was restored (Fig. 8A-peaks 3, 4 and 5). The restoration of the fluorescent emission ensures the detachment of the dye by the metal ions, which proves the sensing ability of the AuNPs towards several cations such as Ca^{2+}, Cu^{2+} and Pb^{2+}.

The addition of metal ions turns-on the fluorescence making a colored highly fluorescent complex (De la Cruz-Guzman, 2014). Therefore, fluorescent enhancement could be attributed to the formation of Rh6G-AuNPs-metal ions complex. Metal ions can either enhance the fluorescence or quench it, but some of them have no effect. For example, Cu^{2+} exhibits a prominent enhancement of the band with a blue-shift (Pal et al., 2014).

Hence, the enhancement of the fluorescence depends of the metal ion nature and the dye. In this case, the Pb^{2+} exhibits the higher enhancement followed by Ca^{2+}, as observed in Fig. 8A. The presence of some metal ions may induce a complementary complex that can recover the fluorescence of the AuNPs2mLCP-Rh6G, these in between complexes turn-on the fluorescence (Guo et al., 2016).

The main difference between LSPR sensing and fluorescence sensing is that LSPR depends directly of the NPs properties, specifically the inter-particle distances and the polarization of the incident light. Meanwhile, in the florescence sensing, it seems to depend on the distance of the fluorophore respect to the surface of the NPs, which determines the effect. Because of these differences, diverse ions are perceived by the studied methods (Langer et al., 2015). Although, it is noteworthy to mention that in both sensing methodologies, Ca^{2+} can be detected relatively easy. It is known that high concentrations of calcium in the body present higher risks of cardiovascular disease (Anderson and Klemmer, 2013). Also, high intakes of calcium, approximately >2500 mg per day, can result in a disease called hypercalcemia, that presents itself with excessive thirst, excessive urination, pain between your back and upper abdomen on one side, arterial calcification, among others (Anderson and Klemmer, 2013). Therefore, the detection of calcium present in the water has a great significance, and the method developed in this work is an excellent alternative to know easily the calcium concentration in water.

It is also important to detect and eliminate other kind of hazardous metals from water such as copper and lead. If a human being ingest an excess of copper, He/She can get a disease called Wilson, affecting the liver and nervous system. Also, lead poisoning can affect the liver, thyroid, hematopoietic and immune systems, among others.

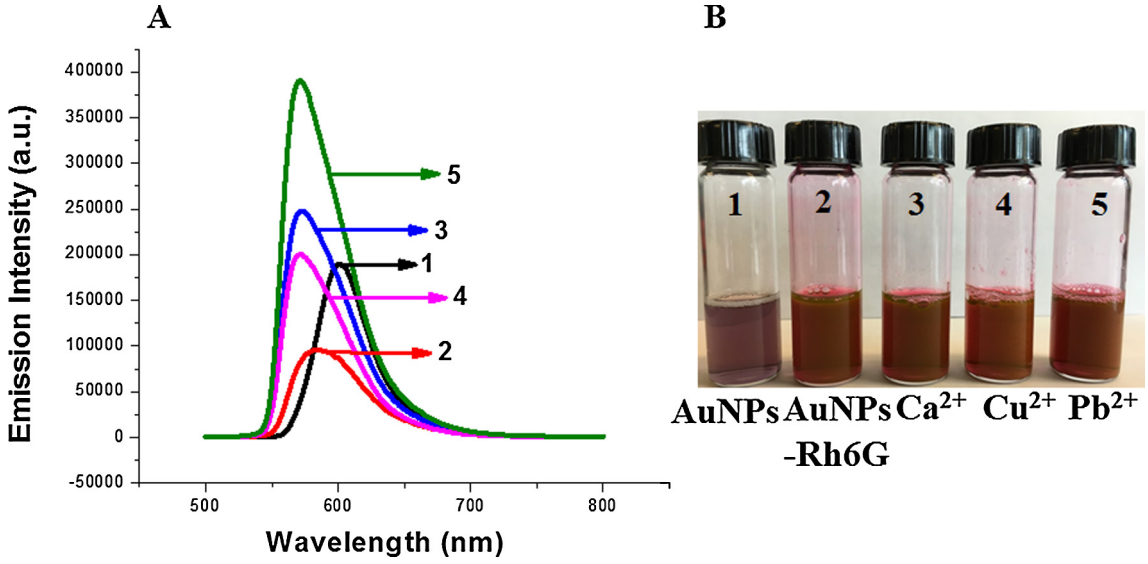

Fig. 8 (A) Fluorescence spectra of biogenic AuNPs obtained with 5 mL of a 10^{-3} M $HAuCl_4$ solution and 2 mL of *Citrus paradisi* aqueous extract as sensors of metal ions with Rhodamine-6G (Rh6G). Spectrum 1 – Rh6G, Spectrum 2 – AuNPs2mLCP-Rh6G, Spectrum 3 – AuNPs2mLCP-Rh6G-Ca^{2+}, Spectrum 4 – AuNPs2mLCP-Rh6G-Cu^{2+}, Spectrum 5 – AuNPs2mLCP-Rh6G-Pb^{2+}. (B) Pictures of biogenic AuNPs solutions of the corresponding spectra 1–5 in (A).

4. Conclusions

The biological synthesis of AuNPs using *Citrus paradisi* extract provides a simple and efficient route for the synthesis of nanomaterials with tunable optical properties directed by shape and size.

During the bioreduction of gold ions, not only the ability of the carboxylic groups in the compounds of the *Citrus paradisi* extract can be associated to the shape-tuning of gold nanotriangles, but also is responsible for the supra-arrangement of gold nanoparticles.

The size of the synthesized Au nanotriangles varied from 25 nm to 325 nm, while the Au nanospheres varied from 5 nm to 85 nm. HRTEM analysis of the sample prepared with 2 mL of *Citrus paradisi* extract shows FCC AuNPs with triangular, hexagonal and spherical shapes. When the amount of extract increased, the shape changes.

AuNPs synthesized by adding 2 mL of *Citrus paradisi* extract possess a unique ability to detect Hg^{2+}, Ca^{2+} and Zn^{2+} through LSPR method. There was no visual color change, but the linear shift in the plasmon absorption was notable. Moreover, fluorescent sensing through fluorescence enhancement opens a new prospect for metal ions sensing, where the bio-synthesized AuNPs had good sensitivity to detect Ca^{2+}, Cu^{2+} and Pb^{2+} in water.

Acknowledgements

This work was Financial Supported by CONACYT – México Grant No. 280518 and UAEM – México Grant Number 1025/2014RIFC. The author Luisa Elena Silva De Hoyos thanks to CONACYT for the Ph. D Grant No. 373046.

References

Ahmed, Shakeel et al, 2016. Green synthesis of silver nanoparticles using *Azadirachta indica* aqueous leaf extract. J. Radiat. Res. Appl. Sci. 9, 1–7.

Ahmed, Shakeel, Ikram, Saiqa, 2015. Synthesis of gold nanoparticles using plant extract: an overview. Nano Res. Appl. 1, 1–5.

Anderson, John J.B., Klemmer, Philip J., 2013. Risk of high dietary calcium for arterial calcification in older adults. Nutrients 5, 3964–3974.

Bankar, Ashok et al, 2010. Banana peel extract mediated synthesis of gold nanoparticles. Colloids Surfaces B: Biointerfaces 80, 45–50.

Das, Vidhya Lakshmi et al, 2014. Extracellular synthesis of silver nanoparticles by the Bacillus strain CS 11 isolated from industrialized area. 3 Biotech 4, 121–126.

Dauthal, Preeti, Mukhopadhyay, Mausumi, 2016. Noble metal nanoparticles: plant mediated synthesis, mechanistic aspects of synthesis and applications. Ind. Eng. Chem. Res. 36, 9557–9577.

De la Cruz-Guzman, Mayela et al, 2014. A turn-on fluorescent solid-sensor for Hg(II) detection. Nanoscale Res. Lett. 9, 2–9.

Ding, Nan et al, 2010. Colorimetric assay for determination of lead (II) based on its incorporation into gold nanoparticles during their synthesis. Sensors 10, 11144–11155.

Gan, Pei Pei, Li, Sam Fong Yau, 2012. Potential of plant as a biological factory to synthesize gold and silver nanoparticles and their applications. Rev. Environ. Sci. Biotechnol. 11, 169–206.

Germain, V. et al, 2003. Stacking faults in formation of silver nanodisks. J. Phys. Chem. B 34, 8717–8720.

Ghashghaei, S., Emtiazi, G., 2015. The methods of nanoparticle synthesis using bacteria as biological nanofactories, their mechanisms and major applications. Curr. Bionanotechnol. 1, 3–17.

Giljohann, David A. et al, 2010. Gold nanoparticles for biology and medicine. Chem. Int. Ed. 49, 3280–3294.

González, A.L. et al, 2005. Optical absorbance of colloidal suspensions of silver polyhedral nanoparticles. J. Phys. Chem. B 109, 17512–17517.

Guo, Yongming et al, 2016. Fluorescent copper nanoparticles: recent advances in synthesis and applications for sensing metal ions. Nanoscale 8, 4852–4863.

Handy, Richard D. et al, 2008. The ecotoxicology and chemistry of manufactured nanoparticles. Ecotoxicology 17, 287–314.

He, Hua, Xie, Chao, Ren, Jicun, 2008. Nonbleaching fluorescence of gold nanoparticles and its applications in cancer cell imaging. Anal. Chem. 80, 15.

Hebbalalu, Deepika et al, 2013. Greener techniques for the synthesis of silver nanoparticles using plant extracts, enzymes, bacteria, biodegradable polymers and microwaves. ACS Sustain. Chem. Eng. 7, 703–712.

Huang, Jiale et al, 2007. Biosynthesis of silver and gold nanoparticles by novel sundried *Cinnamomum camphora* leaf. Nanotechnology 18, 105104.

Jeevanandam, Jaison, Chan, Yen San, Danquah, Michael K., 2016. Biosynthesis of metal and metal oxide nanoparticles. ChemBioEng Rev. 2, 55–67.

Joseph Kirubaharan, C. et al, 2012. Biomediated silver nanoparticles for the highly selective copper (II) ion sensor applications. Ind. Eng. Chem. Res. 51, 7441–7446.

Kang, Kyung A et al, 2011. Fluorescence manipulation by gold nanoparticles: from complete quenching to extensive enhancement. J. Nanobiotechnol. 9, 16.

Krueger, Anke, 2008. Diamond nanoparticles: jewels for chemistry and physics. Adv. Mater. 20, 2445–2449.

Langer, Judith, Novikov, Sergey M., Liz-Marzán, Luis M., 2015. Sensing using plasmonic nanostructures and nanoparticles. Nanotechnology 26, 322001 (28pp).

Lefton, C., Sigmud, W., 2005. Mechanisms controlling crystal habits of gold and silver colloids. Adv. Funct. Mater. 15, 1197–1208.

Li, Xiaomin et al, 2008. Preparation and evaluation of orange peel cellulose adsorbents for effective removal of cadmium, zinc, cobalt and nickel. Colloids Surfaces A: Physicochem. Eng. Aspects 317, 512–521.

Lohse, Samuel E., Murphy, Catherine J., 2012. Applications of colloidal inorganic nanoparticles: from medicine to energy. J. Am. Chem. Soc. 134, 15607–15620.

Mittal, Amit Kumar, Chisti, Yusuf, Banerjee, Uttam Chand, 2013. Synthesis of metallic nanoparticles using plant extracts. Biotechnol. Adv. 31, 346–356.

Montes, M.O. et al, 2011. Anisotropic gold nanoparticles and gold plates biosynthesis using alfalfa extracts. J. Nanopart. Res. 13, 3113–3121.

Nestor, Alfredo Rafael Vilchis, 2006. Síntesis, caracterización y evaluación de las propiedades catalíticas del poli (metacrilato de aluminio (III)). Universidad Autónoma del Estado de México, 103–119.

Niemeyer, Christof M., 2001. Nanoparticles, proteins, and nucleic acids: biotechnology meets materials science. Angew. Chem. Int. Ed. 40, 4128–4158.

Noguez, Cecilia, 2005. Optical properties of isolated and supported metal nanoparticles. Opt. Mater. 27, 1204–1211.

Noguez, Cecilia, 2007. Surface plasmons on metal nanoparticles: the influence of shape and physical environment. J. Phys. Chem. C 111, 3806–3819.

Nolasco-Arizmendi, Víctor et al, 2012. Formation of silk–gold nanocomposite fabric using grapefruit aqueous extract. Textile Res. J. 12, 1229–1235.

Pal, Sanchari, Chatterjee, Nabanita, Bharadwaj, Parimal K., 2014. Selectively sensing first-row transition metal ions through fluorescence enhancement. RSC Adv. 4, 26585.

Pantidos, Nikolaos, Horsfall, Louise E, 2014. Biological synthesis of metallic nanoparticles by bacteria. Fungi Plants. J Nanomed. Nanotechnol. 5, 5.

Petla, Ramesh Kumar et al, 2012. Soybean (Glycine max) leaf extract based green synthesis of palladium nanoparticles. J. Biomater. Nanobiotechnol. 3, 14–19.

Polavarapu, Lakshminarayana et al, 2014. Optical sensing of biological, chemical and ionic species through aggregation of plasmonic nanoparticles. J. Mater. Chem. C 2, 7460.

Prathap Chandran, S. et al, 2006. Synthesis of gold nanotriangles and silver nanoparticles using Aloewera plant extract. Biotechnol. Prog. 22, 577–583.

Prathnaa, N. Chandrasekaran, Raichurb, Ashok M., Mukherjee, Amitava, 2011. Biomimetic synthesis of silver nanoparticles by Citrus limon (lemon) aqueous extract and theoretical prediction of particle size. Colloids Surfaces B: Biointerfaces 82, 152–159.

Romo-Herrera, Jose M., Alvarez-Puebla, Ramon A., Liz-Marzan, Luis M., 2011. Controlled assembly of plasmonic colloidal nanoparticle clusters. Nanoscale 3, 1304–1315.

Salata, O.V., 2004. Applications of nanoparticles in biology and medicine. J. Nanobiotechnol. 2, 1–6.

Sharma, Deepali, Kanchi, Suvardhan, Bisetty, Krishna, 2019. Biogenic synthesis of nanoparticles: a review. Arab. J. Chem. 12(8), 3576–3600.

Shipway, Andrew N. et al, 2000. Investigations into the electrostatically induced aggregation of au nanoparticles. Langmuir 16, 8789–8795.

Shiv Shankar, S. et al, 2004. Biological synthesis of triangular gold nanoprisms. Nat. Mater. 3, 482–488.

Shiv Shankar, S. et al, 2005. Controlling the optical properties of lemongrass extract synthesized gold nanotriangles and potential application in infrared-absorbing optical coatings. Chem. Mater. 17, 566–572.

Sinha, Shelly et al, 2009. Nanoparticles fabrication using ambient biological resources. J. Appl. Biosci. 19, 1113–1130.

Song, Jae Yong, Kim, Beom Soo, 2009. Rapid biological synthesis of silver nanoparticles using plant leaf extracts. Bioprocess Biosyst. Eng. 32, 79–84.

Syed, Asad et al, 2013. Biological synthesis of silver nanoparticles using the fungus Humicola sp. and evaluation of their cytoxicity using normal and cancer cell lines. Spectrochim. Acta Part A: Mol. Biomol. Spectrosc. 114, 144–147.

Wiley, Benjamin et al, 2005. Shape-controlled synthesis of metal nanostructures: the case of silver. Chem.-A Eur. J. 11, 454–463.

Yoosaf, Karuvath et al, 2007. In situ synthesis of metal nanoparticles and selective naked-eye detection of lead ions from aqueous media. J. Phys. Chem. C 111, 12839–12847.

Yue, Guozong et al, 2015. Gold nanoparticles as sensors in the colorimetric and fluorescence detection of chemical warfare agents. Coordinat. Chem. Rev. 15, 30070–30079.